TRMM MICROWAVE IMAGER (TMI) UPDATES FOR FINAL DATA VERSION RELEASE

Rachael Kroodsma[1], Stephen Bilanow[2], Yimin Ji[2], and Darren McKague[3]

[1]ESSIC, University of Maryland / NASA Goddard Space Flight Center
[2]KBRwyle Science Technology and Engineering / NASA Goddard Space Flight Center
[3]University of Michigan

ABSTRACT

The Tropical Rainfall Measuring Mission (TRMM) Microwave Imager (TMI) dataset released by the Precipitation Processing System (PPS) will be updated to a final version within the next year. These updates are based on increased knowledge in recent years of radiometer calibration and sensor performance issues. In particular, the Global Precipitation Measurement (GPM) Microwave Imager (GMI) is used as a model for many of the TMI version updates. This paper discusses four aspects of the TMI data product that will be improved: spacecraft attitude, calibration and quality control, along-scan bias corrections, and sensor pointing accuracy. These updates will be incorporated into the final TMI data version, improving the quality of the data product and ensuring accurate geophysical parameters can be derived from TMI.

***Index Terms*—** Calibration, Microwave radiometry, TRMM, TMI

1. INTRODUCTION

The Tropical Rainfall Measuring Mission (TRMM) had a successful 17+ years of operation that ended in April 2015, carrying the TRMM Microwave Imager (TMI) onboard as one of the primary instruments to measure rainfall. The TMI data product is currently at Version 7 (V7) and will be updated to a final Version 8 (V8) within the next year. There are several modifications that will be incorporated in V8 to improve the TMI calibration and quality of the data product. This paper discusses some of those modifications.

Shortly after TRMM was launched, an extensive post-launch analysis of the TMI data was performed by Wentz *et al.* 2001 [1]. Many of these corrections are still used in the current V7 dataset. However, since then several other radiometers have been launched, leading to a greater understanding of radiometer calibration issues and how to correct for them. Many of the corrections described in this paper are derived based on this knowledge of other radiometers. The Global Precipitation Measurement (GPM) Microwave Imager (GMI), launched in Feb. 2014, has widely been acknowledged as the best calibrated microwave imager [2] and is used as a model for many of the TMI version updates.

Wentz 2015 [3] provides a thorough analysis of the TMI mission data and derives similar corrections to the TMI data as are outlined in this paper. However, the corrections described here will be included in the data version released by the Precipitation Processing System (PPS). Wentz describes corrections to TMI based on the Remote Sensing Systems (RSS) algorithms that are included in the data version released by RSS.

In addition to updating the TMI data product, all spaceborne microwave radiometers with similar channels dating back to 1997 will be incorporated into the GPM mission's constellation of radiometers. Since TMI observations overlap with GMI, TMI can be used to intercalibrate radiometers that were in operation prior to the launch of GPM, resulting in a consistent dataset of observations dating back to 1997. The GPM Intercalibration Working Group (XCAL) is responsible for calculating the intercalibration constants used for the dataset [4].

2. INSTRUMENT DESCRIPTION

TMI is a 9-channel conical scanning radiometer with an offset parabolic reflector at 49° and an approximate Earth-view scan angle of 130° [5]. The design was modeled after the Special Sensor Microwave Imager (SSMI) and includes similar channels to SSMI centered at 19.35, 21.3, 37.0, and 85.5 GHz. In addition, TMI included a lower frequency channel centered at 10.65 GHz to measure heavier rainfall. All channels measure both vertical and horizontal polarization (v/h-pol), except 21.3 GHz which is only v-pol. The 19-85 GHz channels all share a feedhorn, while the 10.65 GHz channels are contained in a separate feedhorn.

3. VERSION UPDATES

The updates to the TMI dataset described here include spacecraft attitude, calibration and quality control, along-scan bias corrections, and sensor pointing accuracy. Other updates that are not discussed here are currently being evaluated by the University of Central Florida. They will provide PPS with antenna pattern corrections and an updated

emissive reflector correction originally derived by Gopalan *et al.* 2009 [6].

3.1. Spacecraft Attitude

The TRMM spacecraft attitude has been recomputed for the entire mission by making use of the onboard Inertial Reference Unit (IRU a.k.a. gyroscope) data, Digital Sun Sensor (DSS) data, and inferred measurements of the spacecraft roll angle using data from the Precipitation Radar (PR) science instrument where available. Previous releases of TRMM products simply used the onboard attitude for geolocation, essentially reporting zero pitch, roll, and yaw since the onboard calculated attitude was also used in the control loop. This generally met the original mission requirements of 0.2° accuracy on all axes, except for occasional excursions and anomalies [7]. By reprocessing the attitudes using the gyroscope data, the spacecraft motions are now tracked reliably to about 0.01° accuracy.

3.2. Calibration and Quality Control

The TMI calibration is improved by implementing a GMI-like scan average calibration. TMI V7 performs a scan-by-scan calibration, where each scan is calibrated using the following hot and cold calibrations. V8 performs a running average of several scans of hot and cold looks which is also done for GMI. This helps to eliminate some of the striping noticed with the previous TMI dataset.

One improvement with TMI quality control is with radio frequency interference (RFI). RFI has become an increasingly prevalent issue for passive sensors, and many current radiometers perform RFI filtering or mitigation as part of quality control. A comprehensive RFI analysis was done with GMI and is used as a model for TMI RFI filtering. RFI in the Earth-view is currently given a flag, while RFI in the cold sky mirror is corrected by using nearby pixels that are clean.

3.3. Along-Scan Bias Correction

The first post-launch analysis of TMI data noticed significant along-scan biases for many of the channels [1]. A simple offset versus scan position correction by channel was implemented to remove the biases in the data product. Over-ocean TAs were averaged using various filters to derive a scan bias as a difference from the mean. This correction assumes that the scan biases are constant at all scene temperatures; however, recent analysis shows that this assumption is not correct.

At a given scan position, the observed TA can be decomposed into the desired on-Earth interference-free main-beam brightness temperature (TB) $T_{b,mb}$, and the contribution from interference/obstruction given the effective brightness of the source of interference $T_{b,i}$ and the effective beam fraction of the interference f_i as: [8]

$$TA = T_{b,mb} * (1 - f_i) + T_{b,i} * f_i \quad (1)$$

Estimating $T_{b,i}$ and f_i at each scan position requires known measurements $T_{b,mb}$. This is done by using over-ocean observations from the vicarious cold calibration technique [9] and over-land observations from the vicarious warm calibration technique [10]. These biases can be linearly interpolated to compute the bias at an arbitrary TA [8,11]. Since beam patterns as well as sources of interference vary from channel to channel, this is done independently for each channel. Fig. 1 shows the TA along-scan biases calculated using the vicarious cold (blue line) and warm (red line) techniques. Both the cold and warm along-scan biases show similar patterns for the large- and small-scale fluctuations, but there are two distinct differences in the biases. One is the edge-of-scan pattern attributed to an obstruction. The second is an overall curvature or slope pattern that is different for cold vs. warm along-scan biases, most notably in the v-pol channels.

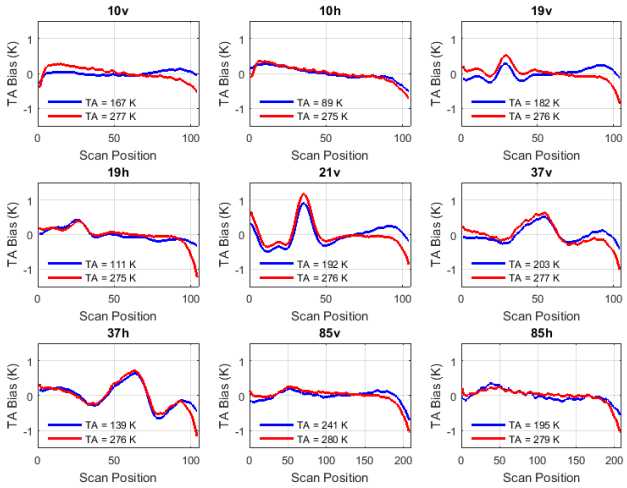

Fig. 1: TMI TA cold and warm along-scan biases calculated using vicarious calibration techniques. The large- and small-scale fluctuations are similar at both TAs, but the edge-of-scan and overall patterns have some significant differences.

One phenomenon that can cause some curvature and/or slope changes across the scan is a pitch and/or roll offset of the spacecraft. Pitch and roll offsets directly affect the earth incidence angle (EIA) of the radiometer, and the cold over-ocean biases are sensitive to EIA variations across the scan while the warm biases are not [12]. Over-ocean v-pol observations are more sensitive than h-pol to EIA differences which is consistent with Fig. 1, where the v-pol cold biases differ more from the warm biases than h-pol. Since the pitch and roll of the spacecraft is accounted for using the method described in Section 3.1, the pitch/roll

offset calculated here is assumed to be an offset of the TMI instrument in relation to the spacecraft. Taking the difference between the cold and warm scan biases for the middle of the scan to remove edge-of-scan effects allows a pitch and roll offset to be calculated from the resulting pattern across the scan. Using the vicarious cold calibration pitch/roll derivation method described in [12], an approximate pitch/roll offset of -0.08º/-0.08º is calculated.

Fig. 2 shows the along-scan bias at both cold and warm TAs, comparing the current V7 biases with V8. The V7 biases are the same for both cold and warm TAs since it is a constant additive bias regardless of scene temperature. The V8 along-scan biases are derived using the vicarious cold and warm techniques, accounting for the pitch/roll offset and calculating a bias at a given scene temperature according to Eq. 1. As seen in Fig. 2, the V8 cold and warm biases have greater agreement for the middle part of the scan compared to Fig. 1, giving us confidence that the correct pitch/roll offset has been applied.

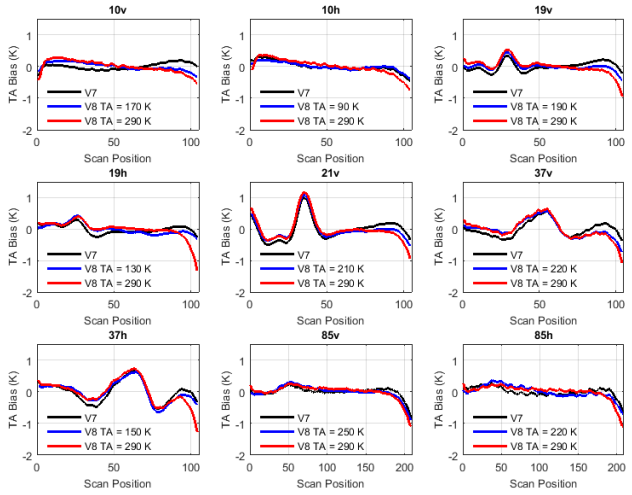

Fig. 2: Comparison of V7 (black), V8 cold (blue), and V8 warm (red) estimates of TMI scan biases. The V7 method assumes these biases are constant as a function of scene temperature, so the new biases can differ significantly at the edge of scan (e.g. ~ 1K right side of 19h scan). The pitch/roll offset included in V8 results in greater agreement between cold and warm biases for the middle of scan.

3.4. Sensor Pointing Accuracy

TMI V7 uses at-launch values for various sensor model parameters to determine geolocation. The TMI instrument field-of-view sweeps a conical path about the instrument spin axis, with a nominal half cone angle of 49°. The start angle for data collection is modeled as -64.4024° relative to the sensor x-axis, and data are collected to approximately +65°. Both the cone angle and start angles are evaluated for modification in V8. Since there are two feedhorns, the 10.65 GHz feedhorn may have a different cone angle and different start angle than the 19-85 GHz feedhorn.

The pointing accuracy of TMI is examined by creating maps of gridded antenna temperatures (TAs) for the two spacecraft yaw orientations. There is a large contrast between land and ocean TAs at microwave imager frequencies, and small offsets in geolocation cause coastlines to appear when taking the difference between the forward and backward looks of TMI. Fig. 3 shows 0.1° gridded Yaw 0 – Yaw 180 TAs for Jan.–Mar. 2004 using V7 geolocation over South America. The coastlines are very apparent in several channels, most notably in 10h. This indicates that the V7 sensor pointing is incorrect and needs to be updated. Since the spacecraft attitude is tracked through the method described in Section 3.1, and the instrument pitch/roll offset is accounted for as described in Section 3.3, a reasonable source of the geolocation error is the cone and start angles. Several Yaw 0 – Yaw 180 TA maps are created using various cone and azimuth start angles and the root mean square (RMS) of the TA variation along the coastline regions is calculated for each case. Table 1 shows the cone and azimuth start angles associated with the minimum RMS for the two feedhorns: (1) 10v/h and (2) 19v/h, 21v, 37v/h, and 85v/h. The constants derived by Wentz 2015 [3] are also reported and we show very similar results. The differences can be attributed to variations in our methods and different spacecraft attitude calculations. Fig. 4 shows the updated TMI geolocation using the new cone and azimuth start angles from Table 1. The pointing accuracy for all channels is greatly improved using the new constants.

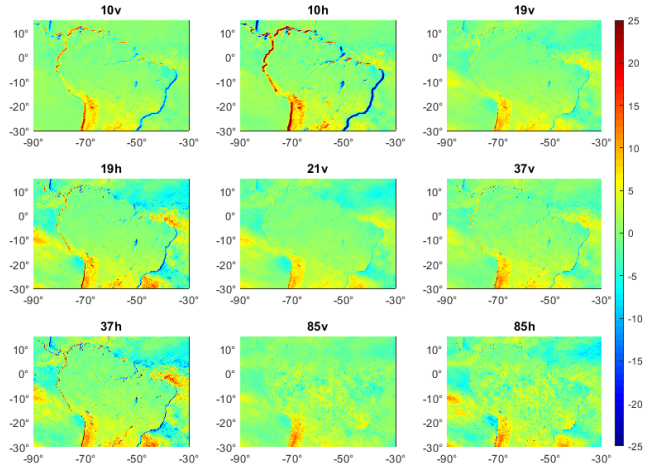

Fig. 3: Yaw 0 – Yaw 180 gridded TMI TAs over South America for V7 geolocation. Incorrect geolocation results in the appearance of coastlines, which can be seen in all channels but is most pronounced in 10h.

Table 1: Cone angles and azimuth start angles calculated for TMI V8 data release, comparing the values derived here (V8) with Wentz 2015 [3].

Channel	Cone Angle (V8)	Cone Angle (Wentz)	Azimuth Start Angle (V8)	Azimuth Start Angle (Wentz)
10v/h	49.45	49.43	-63.91	-63.70
19v – 85h	49.28	49.30	-64.36	-64.10

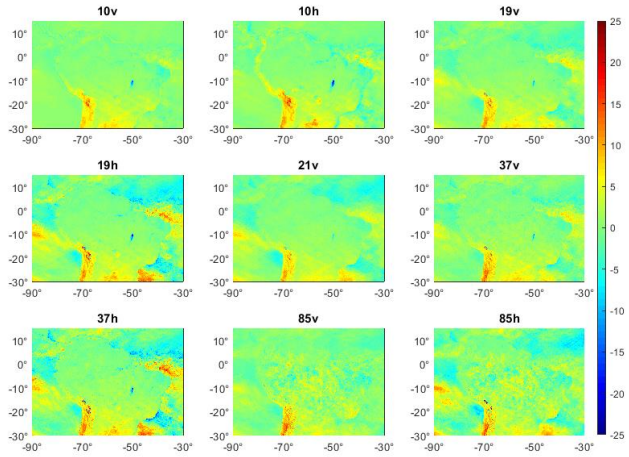

Fig. 4: Yaw 0 – Yaw 180 gridded TMI TAs over South America for updated cone and azimuth start angles to be used in V8. The geolocation for all channels is greatly improved.

4. SUMMARY

The TRMM mission ended in April 2015 after a very successful 17+ years of operation. The TMI data version will be updated to a final version and released within the next year. The updates included in this final version are modeled after successful improvements made to other spaceborne radiometers, with many of the updates modeled after GMI. The improvements described here are the spacecraft attitude, calibration and quality control, along-scan bias corrections, and sensor pointing accuracy. These corrections are important to include in the TMI data product to ensure the accurate retrieval of geophysical parameters.

5. REFERENCES

[1] F. J. Wentz, P. Ashcroft, and C. Gentemann, "Post-Launch Calibration of the TRMM Microwave Imager," *IEEE Trans. Geosci. Rem. Sens.*, 39(2), pp. 415-422, Feb. 2001.

[2] F. J. Wentz, and D. Drape, "On-Orbit Absolute Calibration of the Global Precipitation Measurement Microwave Imager," *J. Atmos. Oceanic Technol.*, pp. 1393-1412, 33, July 2016.

[3] F. J. Wentz, "A 17-Yr Climate Record of Environmental Parameters Derived from the Tropical Rainfall Measuring Mission (TRMM) Microwave Imager," *J. Climate*, 28(17), pp. 6882-6902, Sep. 2015.

[4] W. Berg, *et al.*, "Intercalibration of the GPM Microwave Radiometer Constellation," *J. Atmos. Oceanic Tech.*, 33(12), pp. 2639-2654, Dec. 2016.

[5] C. Kummerow, W. Barnes, T. Kozu, J. Shiue, and J. Simpson, "The Tropical Rainfall Measuring Mission (TRMM) Sensor Package," *J. Atmos. Oceanic Technol.*, 15(3), pp. 809-817, Jun. 1998.

[6] K. Gopalan, W. L. Jones, S. Biswas, S. Bilanow, T. Wilheit, and T. Kasparis, "A Time-Varying Radiometric Bias Correction for the TRMM Microwave Imager," *IEEE Trans. Geosci. Remote Sens.*, 47(11), pp. 3722-3730, Nov. 2009.

[7] S. Bilanow, and S. Slojkowski, "TRMM On-orbit Performance Reassessed after Control Change." *25th Int. Symp. on Space Technology and Science*, Kanazawa City, Japan, ISTS-2006-d-35, June 2016.

[8] D. S. McKague, C. S. Ruf, and J. J. Puckett, "Beam Spoiling Correction for Spaceborne Microwave Radiometers Using the Two-point Vicarious Calibration Method," *IEEE Trans. Geosci. Remote Sens.*, 49(1), pp. 21-27, Jan. 2011.

[9] R. A. Kroodsma, D. S. McKague, and C. S. Ruf, "Vicarious Cold Calibration for Conical Scanning Microwave Imagers," *IEEE Trans. Geosci. Remote Sens.*, 55(2), pp. 816-827, Feb. 2017.

[10] J. X. Yang, D. S. McKague, and C. S. Ruf, "Boreal, Temperate and Tropical Forests as Vicarious Calibration Sites for Spaceborne Microwave Radiometry," *IEEE Trans. Geosci. Remote Sens.*, 54(2), pp. 1035-1051, Feb. 2016.

[11] D. Draper, "Calibration Data Book for Global Precipitation Measurement (GPM) Microwave Imager (GMI)," ed: Ball Aerospace & Technologies Corp, p. 211, 2014.

[12] R. Kroodsma, D. McKague, and C. Ruf, "Satellite Attitude Analysis using the Vicarious Cold Calibration Method for Microwave Radiometers," *Proc. 2012 IEEE International Geoscience and Remote Sensing Symposium*, Munich, Germany, pp. 2964-2967, 23-27 July 2012.